Inorganic Chemistry

Article

pubs.acs.org/IC

Single-Component and Warm-White-Emitting Phosphor $NaGd(WO_4)_2$:Tm^{3+}, Dy^{3+}, Eu^{3+}: Synthesis, Luminescence, Energy Transfer, and Tunable Color

Yan Liu, Guixia Liu,* Jinxian Wang, Xiangting Dong, and Wensheng Yu

Key Laboratory of Applied Chemistry and Nanotechnology at Universities of Jilin Province, Changchun University of Science and Technology, Weixing Road No. 7989, Changchun 130022, China

ABSTRACT: Tm^{3+}, Dy^{3+}, and Eu^{3+} codoped $NaGd(WO_4)_2$ phosphors were prepared by a facile hydrothermal process; they were characterized by X-ray diffraction (XRD), field emission scanning electron microscope (FESEM), energy-dispersive X-ray spectrometer (EDS), photoluminescence spectra, and fluorescence lifetime. The results show that the novel octahedral microcrystals with a mean side length of 2 μm are obtained. Under the excitation of ultraviolet, individual RE^{3+} ion (Tm^{3+}, Dy^{3+}, and Eu^{3+}) activated $NaGd(WO_4)_2$ phosphors exhibit excellent emission properties in their respective regions. Moreover, when codoping Dy^{3+} and Eu^{3+}/Tm^{3+} in the single component, the energy migration from Dy^{3+} to Eu^{3+} has been demonstrated to be a resonant type via a dipole−quadrupole mechanism as well as that from Tm^{3+} to Dy^{3+} ions, of which the critical distance (R_{Dy-Eu}) is calculated to be 11.08 Å. More significantly, in the Tm^{3+}, Dy^{3+}, and Eu^{3+} tridoped $NaGd(WO_4)_2$ phosphors, the energy migration of Tm^{3+}−Dy^{3+}−Eu^{3+}, utilized for sensitizing Eu^{3+} ions besides compensating the red component at low Eu^{3+} doping concentration, has been discussed first. In addition, under 365 nm near-ultraviolet radiation (nUV), the color-tunable emissions in octahedral $NaGd(WO_4)_2$ microcrystals are realized by giving abundant blue, green, white, yellow, and red emissions, especially warm white emission, and could be favorable candidates in full-color phosphors for nUV-LEDs.

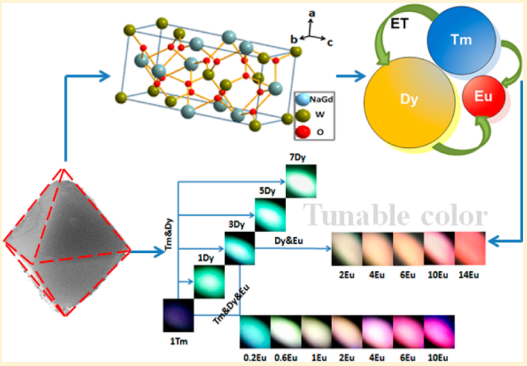

1. INTRODUCTION

As the hot spot in solid-state lighting areas, white light-emitting diodes (WLEDs) have attracted considerable attention as the next generation lighting source due to their attractive features such as excellent luminescent characteristics, good stability, high luminescence efficiency, as well as low cost.[1−3] At present, conventional WLEDs coupling a blue GaN LED chip with commercial yellow-emitting phosphors (YAG:Ce) exhibit an unsatisfactory high correlated color temperature (CCT ≈ 7750 K) and low color-rendering index (CRI ≈ 70−80) due to the deficiency of the red emission, which restricts their use in more vivid applications.[4,5] Therefore, the general lack of red emitting that can improve the performance of white light in terms of color-rendering has become one of the key factors limiting the progress of WLEDs. In order to upgrade the behavior of white light with a high color-rendering index, a red component, specifically as a result of the red emitting from Eu^{3+}, Sm^{3+}, and Mn^{2+}, is indispensably introduced into the system, such as tricolor single-component inorganic phosphors combining with multicolor emission bands of rare earth ions pumped by UV or near-UV LED chips. Warm light emitting has been successfully obtained through that method in $NaLa(WO_4)_2$:Tm^{3+}/Tb^{3+}/Eu^{3+},[6] $KSr_4(BO_3)_3$/YVO_4:Tm^{3+}/Dy^{3+}/Eu^{3+},[7,8] $Na_2Y_2B_2O_7$:Ce^{3+}/Tb^{3+}/Eu^{3+},[9] $YP_xV_{1-x}O_4$:Dy^{3+}/Sm^{3+},[10] $Ca_5(PO_4)_2SiO_4$/$Sr_{3.5}Y_{6.5}O_2(PO_4)_{1.5}(SiO_4)_{4.5}$:$Ce^{3+}$/$Tb^{3+}$/$Mn^{2+}$,[11,12] and $Sr_{10}[(PO_4)_{5.5}(BO_4)_{0.5}](BO_2)$:$Eu^{2+}$/$Tb^{3+}$/$Mn^{2+}$.[13] Additionally, significant efforts have been recently advanced in the field of MOFs (metal organic framework) as an attractive alternative to single component warm white light emitters, whose photoluminescence is tunable through metal and organic ligand substitutions.[14−16]

As one of the most frequently used red emitters in rare earth ions doped materials, the Eu^{3+} mainly presents high efficiency characteristic emissions related to the large energy gap between the emitting state $^5D_{0,1,2}$ and the excited states ^7F_J (J = 1, 2, 3, 4, 5) for offering intense red composition.[17] Moreover, taking account of the Dy^{3+} $^4F_{9/2} \rightarrow {}^6H_{15/2}$ and $^4F_{9/2} \rightarrow {}^6H_{13/2}$ emissions in the blue and yellow regions, respectively, it is of interest to produce Dy^{3+}-activated white phosphors due to the combination of blue and yellow emissions. Nevertheless, the Dy^{3+} single-doped phosphor suffers from a lack of red component generating cold white light.[18] Thus, it is necessary to compensate the red component; Eu^{3+} ions are added into the same host lattice. In addition, it is noteworthy that extensive investigation of LED phosphor has been underway in recent years, in which codoping a sensitizer and an activator into the same host is an efficient way to produce white emission by controlling the energy transfer between sensitizers and activators. Remarkably, the energy

Received: June 2, 2014
Published: October 10, 2014

   dx.doi.org/10.1021/ic501284y | Inorg. Chem. 2014, 53, 11457−11466

transfer process from Dy^{3+} to Eu^{3+} has been investigated in some inorganic hosts, such as SrY_2O_4,[18] Y_2O_2S,[19] and $YP_xV_{1-x}O_4$.[10]

Meanwhile, Tm^{3+} ions, usually used as efficient blue light emissive activators, have blue emissions mainly assigned to $^1D_2 \rightarrow {}^3F_4$ transition of Tm^{3+} ions, which overlaps well with the $^6H_{15/2} \rightarrow {}^4I_{15/2}$ transition of Dy^{3+}. The Tm^{3+} sensitization effect has been utilized to sensitize Dy^{3+} ion emission in previous reports,[7,8,20,21] where multicolor and cold white light were obtained used for WLEDs as well as some reports about Tm^{3+} and Dy^{3+} codoping white phosphors in field emission displays.[22,23] In Wu's and Luwang's reports,[7,8] Tm^{3+}, Dy^{3+}, and Eu^{3+} tunable phosphors had been previously obtained and exhibited desirable properties. However, in both cases, properties of Eu^{3+} ions were merely used as the supplier of red component without the investigation of total energy transfer process among Tm^{3+}, Dy^{3+}, and Eu^{3+} ions in the tridoped phosphors. Recently, the energy transfer processes of $Ce^{3+}-(Tb^{3+})_n-Eu^{3+}$ and $Eu^{2+}-(Tb^{3+})_n-Eu^{3+}$ have been successfully put forward to sensitize Eu^{3+} ions and realize the narrow-line red emission with near UV broad band excitation in $Y_2SiO_5/Na_2Y_2B_2O_7:Ce^{3+}$, Tb^{3+}, Eu^{3+},[9,24] $Ba_2(Ln_{1-z}Tb_z)(BO_3)_2Cl:Eu^{2+}$, Eu^{3+}.[25] However, to our knowledge, no system based on the energy transfer of $Tm^{3+}-Dy^{3+}-Eu^{3+}$ ions is yet known.

In this work, we aim to focus our attention on $NaGd(WO_4)_2$ (hereafter referred to as NGW) as a host, and Dy^{3+}, Eu^{3+}, and Tm^{3+} ions as activated ions. Dy^{3+} and Eu^{3+} ions codoped, Tm^{3+} and Dy^{3+} ions codoped, and Tm^{3+}, Dy^{3+}, Eu^{3+} tridoped NGW phosphors are prepared by a simple hydrothermal method. A series of white emitting phosphors based on the efficient $Dy^{3+}-Eu^{3+}$, $Tm^{3+}-Dy^{3+}$, and $Tm^{3+}-Dy^{3+}-Eu^{3+}$ resonance-type energy transfer processes are realized. We have penetrated the related energy transfer mechanism between the luminescence centers Tm^{3+} and Dy^{3+} as well as Eu^{3+} ions. These phosphors are shown to be suitably color-tunable and are warm white phosphors for UV or near-UV WLEDs.

2. EXPERIMENTAL SECTION

2.1. Materials. Aqueous solutions of $Gd(NO_3)_3$, $Tm(NO_3)_3$, $Dy(NO_3)_3$, and $Eu(NO_3)_3$ were obtained by dissolving the rare earth oxides Ln_2O_3 (Ln = Gd, Tm, Dy, Eu) (99.99%) in dilute HNO_3 solution (15 mol/L) under heating with agitation in ambient atmosphere. All the other chemicals were of analytic grade and used as received without further purification.

2.2. Preparation. A series of rare-earth-doped $NaGd(WO_4)_2$ phosphors were synthesized by a facile hydrothermal process without further sintering treatment. A 1.0 mmol portion of $RE(NO_3)_3$ [including $Gd(NO_3)_3$, $Tm(NO_3)_3$, $Dy(NO_3)_3$, or $Eu(NO_3)_3$] was added into a 100 mL flask. After vigorous stirring for 20 min, 2.0 mmol of $Na_2WO_4{\cdot}2H_2O$ was slowly added dropwise into the above solution. After additional agitation for 30 min, the resultant milky colloidal suspension was transferred to a Teflon bottle held in a stainless steel autoclave, and then heated at 180 °C for 20 h. Finally, as the autoclave was naturally cooled to room temperature, the precipitates were separated by centrifugation, washed with deionized water and ethanol in sequence each several times, and then dried in air at 60 °C for 12 h. Specific material formula is shown in Table 1.

2.3. Characterization. The purity and phase structure of the products were examined by X-ray powder diffraction (XRD) performed on a Rigaku D/max-RA X-ray diffractometer with Cu Kα radiation (λ = 0.154 06 nm) and Ni filter, operating at 20 mA, 30 kV. Scanning speed, step length, and diffraction range were 10°/min, 0.1°, and 10−90°, respectively. The morphology and composition of the samples were observed by a FEI XL-30 field emission scanning electron microscope (FESEM) equipped with an energy-dispersive X-ray spectrometer (EDS). The excitation and emission spectra and the luminescence decay curves of samples were recorded with a HITACHI F-7000 fluorescence spectrophotometer using a Xe lamp as the excitation source, scanning at 1200 nm/min.

Table 1. Specific Material Formula of NGW:Tm^{3+}, Dy^{3+}, Eu^{3+} Samples

	proportion of $RE(NO_3)_3$ (%)			
sample	Gd	Tm	Dy	Eu
NGW:0.03Dy^{3+}	97		3	
NGW:0.03Dy^{3+}, 0.02Eu^{3+}	95		3	2
NGW:0.03Dy^{3+}, 0.04Eu^{3+}	93		3	4
NGW:0.03Dy^{3+}, 0.06Eu^{3+}	91		3	6
NGW:0.03Dy^{3+}, 0.10Eu^{3+}	87		3	10
NGW:0.03Dy^{3+}, 0.14Eu^{3+}	83		3	14
NGW:0.01Tm^{3+}	99	1		
NGW:0.01Tm^{3+}, 0.01Dy^{3+}	98	1	1	
NGW:0.01Tm^{3+}, 0.03Dy^{3+}	96	1	3	
NGW:0.01Tm^{3+}, 0.05Dy^{3+}	94	1	5	
NGW:0.01Tm^{3+}, 0.07Dy^{3+}	92	1	7	
NGW:0.005Tm^{3+}, 0.03Dy^{3+}	96.5	0.5	3	
NGW:0.01Tm^{3+}, 0.03Dy^{3+}	96	1	3	
NGW:0.03Tm^{3+}, 0.03Dy^{3+}	94	3	3	
NGW:0.05Tm^{3+}, 0.03Dy^{3+}	92	5	3	
NGW:0.07Tm^{3+}, 0.03Dy^{3+}	90	7	3	
NGW:0.01Tm^{3+}, 0.03Dy^{3+}, 0.002Eu^{3+}	95.8	1	3	0.2
NGW:0.01Tm^{3+}, 0.03Dy^{3+}, 0.006Eu^{3+}	95.4	1	3	0.6
NGW:0.01Tm^{3+}, 0.03Dy^{3+}, 0.01Eu^{3+}	95	1	3	1
NGW:0.01Tm^{3+}, 0.03Dy^{3+}, 0.04Eu^{3+}	92	1	3	4
NGW:0.01Tm^{3+}, 0.03Dy^{3+}, 0.06 Eu^{3+}	90	1	3	6
NGW:0.01Tm^{3+}, 0.03Dy^{3+}, 0.10Eu^{3+}	86	1	3	10

3. RESULTS AND DISCUSSION

3.1. Crystallization Behavior and Structure. The XRD patterns of $NaGd(WO_4)_2$ phosphors have been shown in Figure

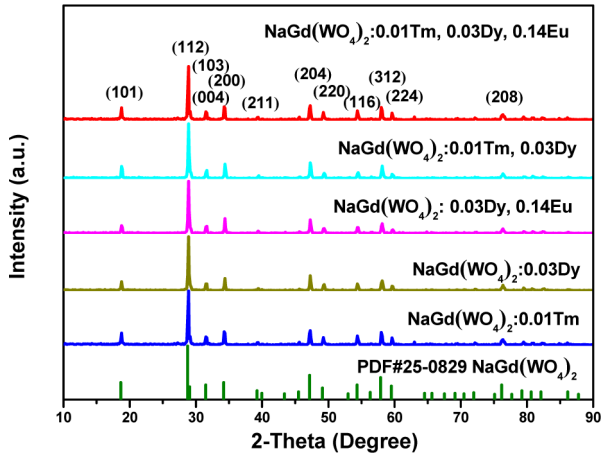

Figure 1. X-ray powder diffraction patterns of NGW:Tm^{3+}, Dy^{3+}, Eu^{3+}.

1. All the diffraction peaks of these samples can be assigned to pure tetragonal phase of $NaGd(WO_4)_2$ with $I4_1/a$ (No. 88), and they match well with the standard values of PDF card (no. 25-0829) indicating that the doped Tm^{3+}, Dy^{3+}, Eu^{3+} ions have no impact on the host structure. The $NaGd(WO_4)_2$ compound belongs to $CaWO_4$ type structure, which has the cell parameters of $a = b = 5.243$ Å, $c = 11.368$ Å, and $Z = 4$. The crystal structure of $NaGd(WO_4)_2$ is shown in Figure 2a. As shown in Figure 2a, there are two crystallographic positions of cations in the unit cell:

dx.doi.org/10.1021/ic501284y | Inorg. Chem. 2014, 53, 11457−11466

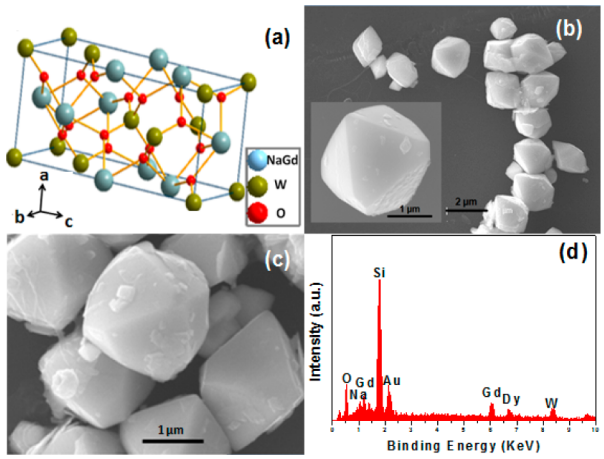

Figure 2. Crystal structure of NGW (a), FESEM images (b,c) and EDS pattern (d) of NGW:Dy^{3+} phosphor.

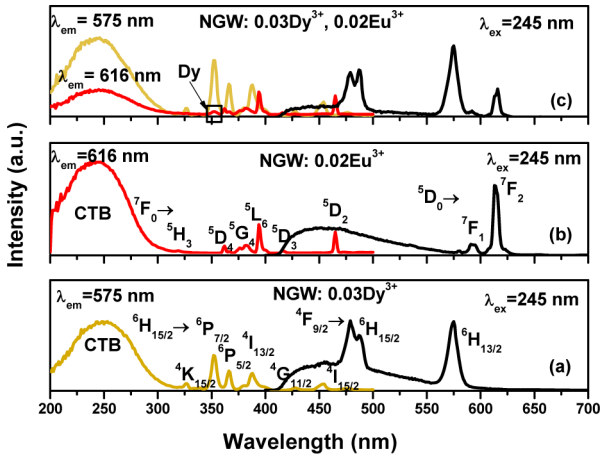

Figure 3. PL and PLE spectra for NGW:0.03Dy^{3+} (a), NGW:0.02Eu^{3+} (b), and NGW:0.03Dy^{3+}, 0.02Eu^{3+} (c) phosphors.

8-fold coordinated Na^+ sites and 8-fold coordinated Gd^{3+} sites. According to the effective ionic radii of cations, the rare earth ions are proposed to occupy the Gd^{3+} sites or Na^+ sites, because the effective radii of Tm^{3+} ions (1.134 Å for CN = 8), Dy^{3+} ions (1.167 Å for CN = 8), and Eu^{3+} ions (1.066 Å for CN = 8) are highly close to those of both Gd^{3+} ions (1.193 Å for CN = 8) and Na^+ ions (1.18 Å for CN = 8). However, on the basis of the valence state analysis, the rare earth ions are much more probably occupying the Gd^{3+} sites. The morphological features and composition of the NGW:Dy^{3+} phosphor were investigated by EFSEM and EDS, as shown in Figure 2b,c and Figure 2d. It can be seen that the NGW:Dy^{3+} phosphor exhibits octahedral microcrystal with a mean side length of 2 μm. The EDS pattern provides the chemical composition of the product, containing Na, Gd, Eu, W, and O (silicon and gold signals are from silicon host and spraying gold process). Combined with above XRD patterns, the samples are further proven to be $NaGd(WO_4)_2$.

3.2. Photoluminescence Properties of $NaGd(WO_4)_2$:Dy^{3+}, Eu^{3+} Phosphors. Figure 3 illustrates the room temperature photoluminescence excitation and emission spectra for NGW:0.03Dy^{3+} (a), NGW:0.02Eu^{3+} (b), and NGW:0.03Dy^{3+}, 0.02Eu^{3+} (c). As depicted in Figure 3a, it can be seen that, in the PLE spectrum monitoring the yellow emission of Dy^{3+} (575 nm, $^4F_{9/2} \rightarrow {}^6H_{13/2}$), the overall excitation spectrum can be divided into two parts: one is a charge transfer band (CTB) centered at 245 nm from 200 to 320 nm, which is attributed to the O^{2-}–W^{6+} charge transfer within the WO_4^{2-} groups. The other is composed of a series of narrow bands from 320 to 500 nm, which correspond to the characteristic f–f transitions ($^6H_{15/2} \rightarrow {}^6P_{7/2}$ at 353 nm, $^6H_{15/2} \rightarrow {}^6P_{5/2}$ at 366 nm, $^6H_{15/2} \rightarrow {}^4I_{13/2}$ at 388 nm, $^6H_{15/2} \rightarrow {}^4G_{11/2}$ at 428 nm, and $^6H_{15/2}$

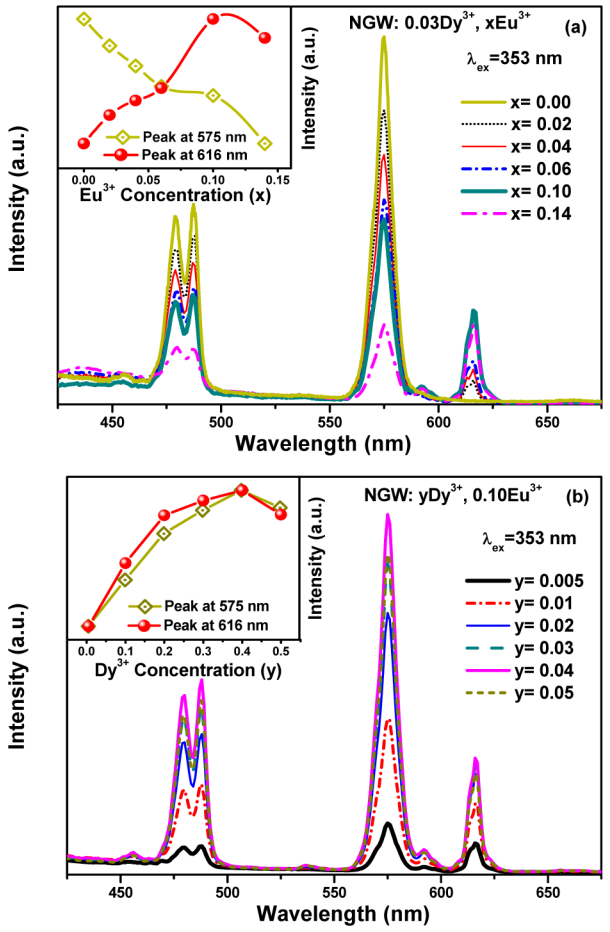

Figure 4. PL spectra for NGW:0.03Dy^{3+}, $x$$Eu^{3+}$ phosphors with different Eu^{3+} doped concentrations (x) (a) and NGW:$y$$Dy^{3+}$, 0.10$Eu^{3+}$ with different Dy^{3+} doped concentrations (y) (b). Inset shows dependence of the emission intensity at different wavelengths on Eu^{3+}/Dy^{3+} concentrations.

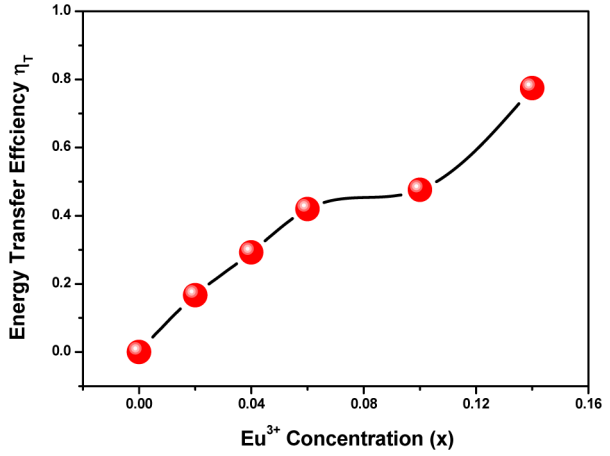

Figure 5. Dependence of energy transfer efficiency η_T on Eu^{3+} concentration in NGW:0.03Dy^{3+}, $x$$Eu^{3+}$ phosphors.

dx.doi.org/10.1021/ic501284y | Inorg. Chem. 2014, 53, 11457–11466

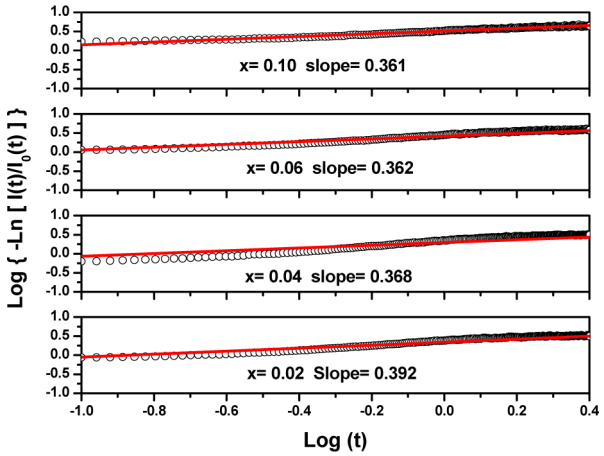

Figure 6. Experimental data plots of $\log\{-\ln[I(t)/I_0(t)]\}$ versus $\log(t)$ of Dy^{3+} in the NGW:Dy^{3+}, Eu^{3+} phosphors. The red lines indicate the fitting behaviors.

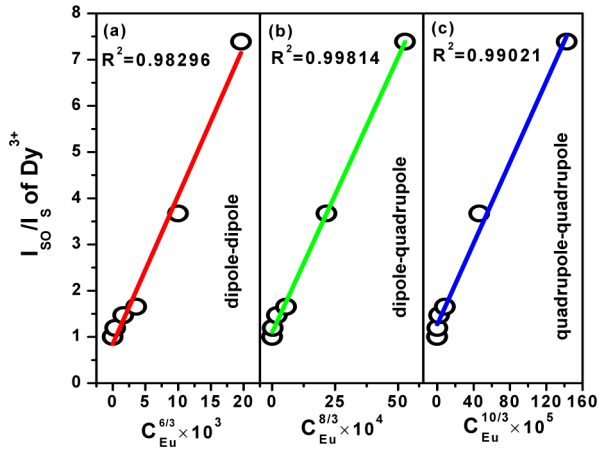

Figure 7. Dependence of I_{so}/I_s of Dy^{3+} on (a) $C_{Eu}^{6/3} \times 10^2$, (b) $C_{Eu}^{8/3} \times 10^5$, and (c) $C_{Eu}^{10/3} \times 10^6$ in the NGW:0.03Dy^{3+}, $x$$Eu^{3+}$ phosphors.

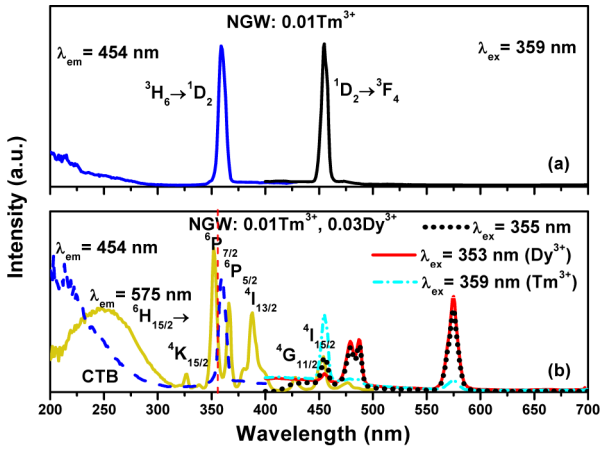

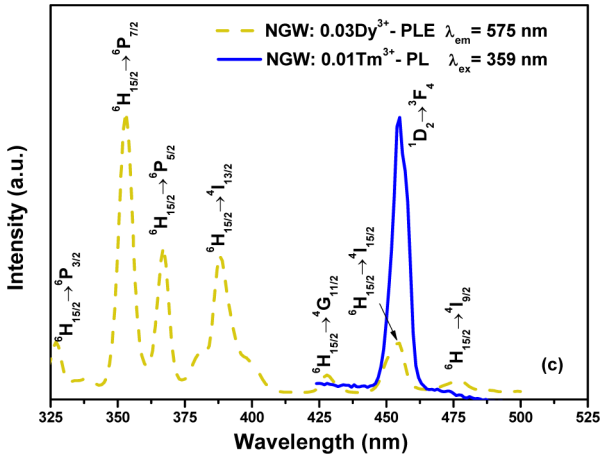

Figure 8. PL and PLE spectra for NGW:0.01Tm^{3+} (a) and NGW:0.01Tm^{3+}, 0.03Dy^{3+} (b) phosphors; overlapping of Tm^{3+} PL spectrum for NGW:0.01Tm^{3+} and the Dy^{3+} PLE spectrum for NGW:0.03Dy^{3+} (c).

→ $^4I_{15/2}$ at 455 nm) for Dy^{3+} ions. Under 245 nm excitation, NGW:0.03Dy^{3+} phosphor obtains blue and yellow luminescence, corresponding to the magnetic dipole $^4F_{9/2} \rightarrow {}^6H_{15/2}$ (478 and 488 nm) and the electric dipole $^4F_{9/2} \rightarrow {}^6H_{13/2}$ (575 nm), characteristic emissions of Dy^{3+} ions.

When monitoring by the red emission of Eu^{3+} (616 nm, $^5D_0 \rightarrow {}^7F_2$), the PLE spectrum of NGW:0.02Eu^{3+} exhibits some peaks at 323, 364, 385, 395, 416, 466 nm corresponding to the transitions of Eu^{3+} ion from the ground level $^7F_0$ to the $^5H_3$, $^5D_4$, $^5L_7$, $^5L_6$, $^5D_3$, and $^5D_2$ excited levels, respectively,[26] simultaneously including a broad absorption band assigned to CTB of WO_4^{2-} groups and O^2–Eu^{3+} charge transfer transition from an oxygen 2p state excited to an Eu^{3+} 4f state.[27] The PL spectrum of NGW:0.02Eu^{3+} phosphor is obtained by exciting at 245 nm. The transition band of $^5D_0 \rightarrow {}^7F_2$ at 616 nm is due to electric dipole transition, which is dominant over other transitions in all the cases, whereas that of $^5D_0 \rightarrow {}^7F_1$ at 593 nm is due to magnetic dipole transition (Figure 3b). Generally, the intensity ratio of the electric dipole to magnetic dipole transitions is used to determine the symmetry of the local environment.[15] In NGW:Eu^{3+}, the intensity of electric transition of the Eu^{3+} ions is almost 7 times more intense than that of the magnetic dipole transition, intimating that the Eu^{3+} ions occupy the low symmetry sites. Thus, the red emission is often dominant in the emission spectrum.

As shown in Figure 3a,b, the comparison between the PLE spectra of NGW:0.03Dy^{3+} and NGW:0.02Eu^{3+} reveals that there are some excitation peaks from 350 to 420 nm of Dy^{3+} and Eu^{3+} ions, indicating that those phosphors can match well with the emission light of UV-LED chips. In addition, the presence of the excitation band of WO_4^{2-} groups and overlaps between the emission band of WO_4^{2-} and the excitation peaks of Dy^{3+} or Eu^{3+} ions prove the existence of energy transfer from WO_4^{2-} to Dy^{3+} and Eu^{3+}.

In Figure 3c, one can observe a manifest $^6H_{15/2} \rightarrow {}^6P_{7/2}$ (353 nm) transition of Dy^{3+} when monitoring by the $^5D_0 \rightarrow {}^7F_2$ emission of Eu^{3+} ions at 616 nm for NGW:0.03Dy^{3+}, 0.02Eu^{3+} indicating the energy migration from Dy^{3+} to Eu^{3+}. The excitation into the PLE band of WO_4^{2-} groups at 245 nm yields the emission of both Dy^{3+} and Eu^{3+} ions, which consists of blue and yellow bands corresponding to the f–d transition ($^4F_{9/2} \rightarrow {}^6H_{15/2}$ and $^4F_{9/2} \rightarrow {}^6H_{13/2}$) for Dy^{3+} ions and a kenspeckle red band attributed to the $^5D_0$–$^7F_2$ transition of the Eu^{3+} ions, respectively. Therefore, warm white light emission can be realized by combining the emission of the Dy^{3+} and Eu^{3+} ions in a single host under UV light excitation by properly tuning the amount of the Eu^{3+} ions through the principle of energy transfer.

Therefore, a series of NGW:0.03Dy^{3+}, $x$$Eu^{3+}$ (x = 0.00, 0.02, 0.04, 0.06, 0.10, 0.14) and NGW:$y$$Dy^{3+}$, 0.10$Eu^{3+}$ (y = 0.005,

dx.doi.org/10.1021/ic501284y | Inorg. Chem. 2014, 53, 11457–11466

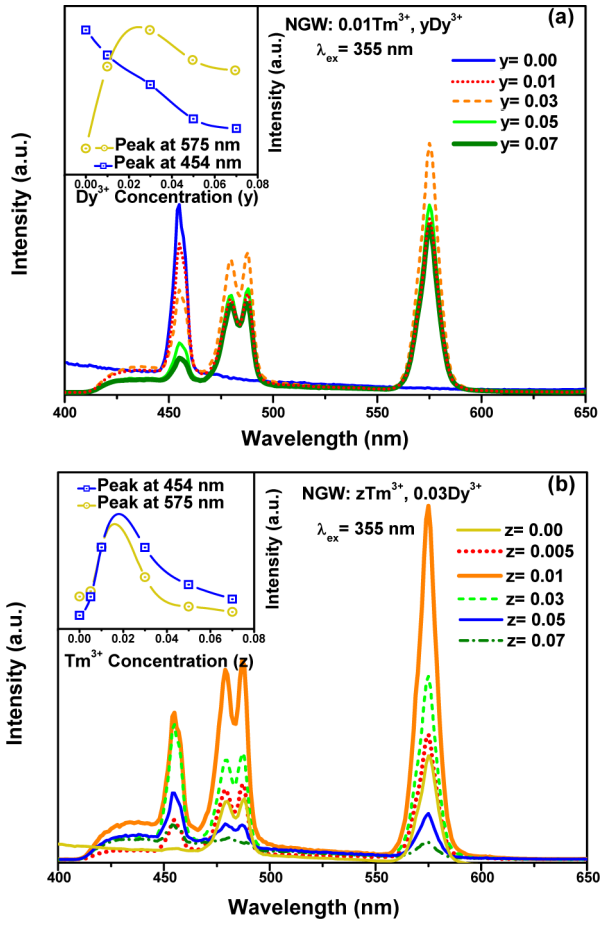

Figure 9. PL spectra for NGW:0.01Tm^{3+}, $y$$Dy^{3+}$ phosphors with different Dy^{3+} doped concentrations (y) (a) and NGW:$z$$Tm^{3+}$, 0.03$Dy^{3+}$ phosphors with different Tm^{3+} doped concentrations (z) (b). Inset shows dependence of the emission intensity at different wavelengths on Dy^{3+}/Tm^{3+} concentrations.

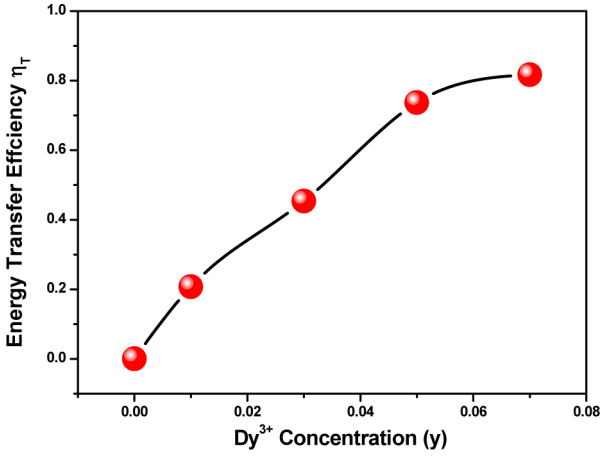

Figure 10. Dependence of energy transfer efficiency η_T on Dy^{3+} concentration in NGW:0.01Tm^{3+}, $y$$Dy^{3+}$ phosphors.

0.01, 0.02, 0.03, 0.04, 0.05) samples have been prepared. The PL spectra of the as-prepared samples with 353 nm excitation are presented in Figure 4a,b. As shown in Figure 4a, the Eu^{3+} concentration is varied, whereas that of Dy^{3+} is fixed at 0.03. The intensity of the Dy^{3+} emission decreases with increasing Eu^{3+} concentration. In addition, Figure 4b depicts the PL spectra of

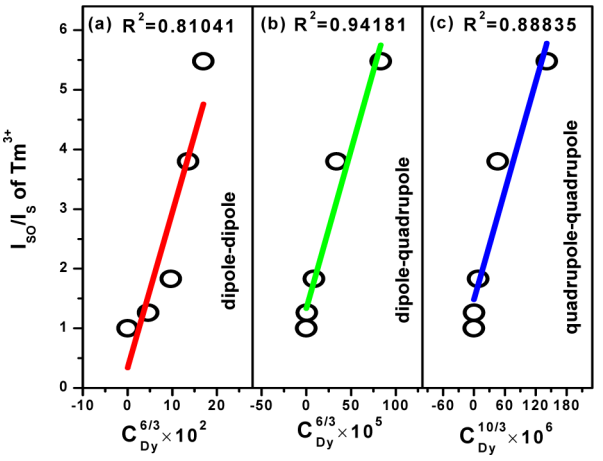

Figure 11. Dependence of I_{so}/I_s of Tm^{3+} on (a) $C_{Dy}^{6/3} \times 10^2$, (b) $C_{Dy}^{8/3} \times 10^5$, and (c) $C_{Dy}^{10/3} \times 10^6$ in the NGW:Tm^{3+}, Dy^{3+} phosphors.

NGW:$y$$Dy^{3+}$, 0.10$Eu^{3+}$ phosphors with y varying from 0.005 to 0.05. Although the Eu^{3+} ion concentration is fixed, the emission intensity of Eu^{3+} ions demonstrably increased at a certain range. The relative emission intensities of Dy^{3+} ions at 575 nm and Eu^{3+} ions at 616 nm as a function of Eu^{3+} concentration are shown in Figure 4, inset. The above variations in the emission intensities of the Dy^{3+} and Eu^{3+} ions strongly prove the occurrence of the energy transfer from Dy^{3+} to Eu^{3+} ions.

The energy-transfer efficiencies (η_T) from Dy^{3+} to Eu^{3+} are calculated using the following formula[28]

$$\eta_T = 1 - I/I_0 \quad (1)$$

where I and I_0 are the intensities of donors with and without the acceptor ions. The energy transfer efficiency is calculated as a function of Eu^{3+} concentration and is shown in Figure 5. The efficiency η_T increases gradually and reaches approximatively 80% at x = 0.14. The reason is that the probability of the energy transfer from Dy^{3+} to Eu^{3+} is proportional to R^{-S} (R is the average distance between Dy^{3+} and Eu^{3+}, S = 6, 8, and 10 correspond to resonant energy transfer mechanism between Dy^{3+} and Eu^{3+} ions: dipole−dipole, dipole−quadrupole, and quadrupole−quadrupole interactions, respectively). Moreover, the critical distance R_{Dy-Eu} of energy transfer from Dy^{3+} to Eu^{3+} can be calculated using the concentration quenching method[29]

$$R_{Dy-Eu} = 2 \times [3V/(4\pi x_c Z)]^{1/3} \quad (2)$$

where V is the volume of the unit cell, x is the total concentration of activator ions, and Z is the number of available crystallographic sites occupied by the activator ions in the unit cell. For the NGW host lattice, V = 304.8 $Å^3$ and Z = 4. The critical concentration x_c, at which the luminescence intensity of Dy^{3+} is half of that in the absence of Eu^{3+}, is 0.107. Therefore, the critical distance (R_{Dy-Eu}) of energy transfer is calculated to be about 11.08 Å. With the enhancement of Eu^{3+} concentration, the distance between Dy^{3+} and Eu^{3+} becomes small enough (shorter than 11.08 Å), so the following resonant energy transfer occurs: the $^4F_{9/2}$ (2.54 eV) level of Dy^{3+} overlaps well with the $^5D_1$ (2.28 eV) and $^5D_0$ (2.01 eV) levels of Eu^{3+}, courting the occurrence of the nonradiative relaxation from $^4F_{9/2}$ level of Dy^{3+} to the $^5D_1$ and $^5D_0$ levels of Eu^{3+}. Thus, the energy transfer also occurs between Dy^{3+} and Eu^{3+} through the cross-relaxation process (Figure 13).

In order to analyze the energy transfer mechanism, we employ the Inokuti−Hirayama (I−H) model to deal with the fluorescent

dx.doi.org/10.1021/ic501284y | Inorg. Chem. 2014, 53, 11457−11466

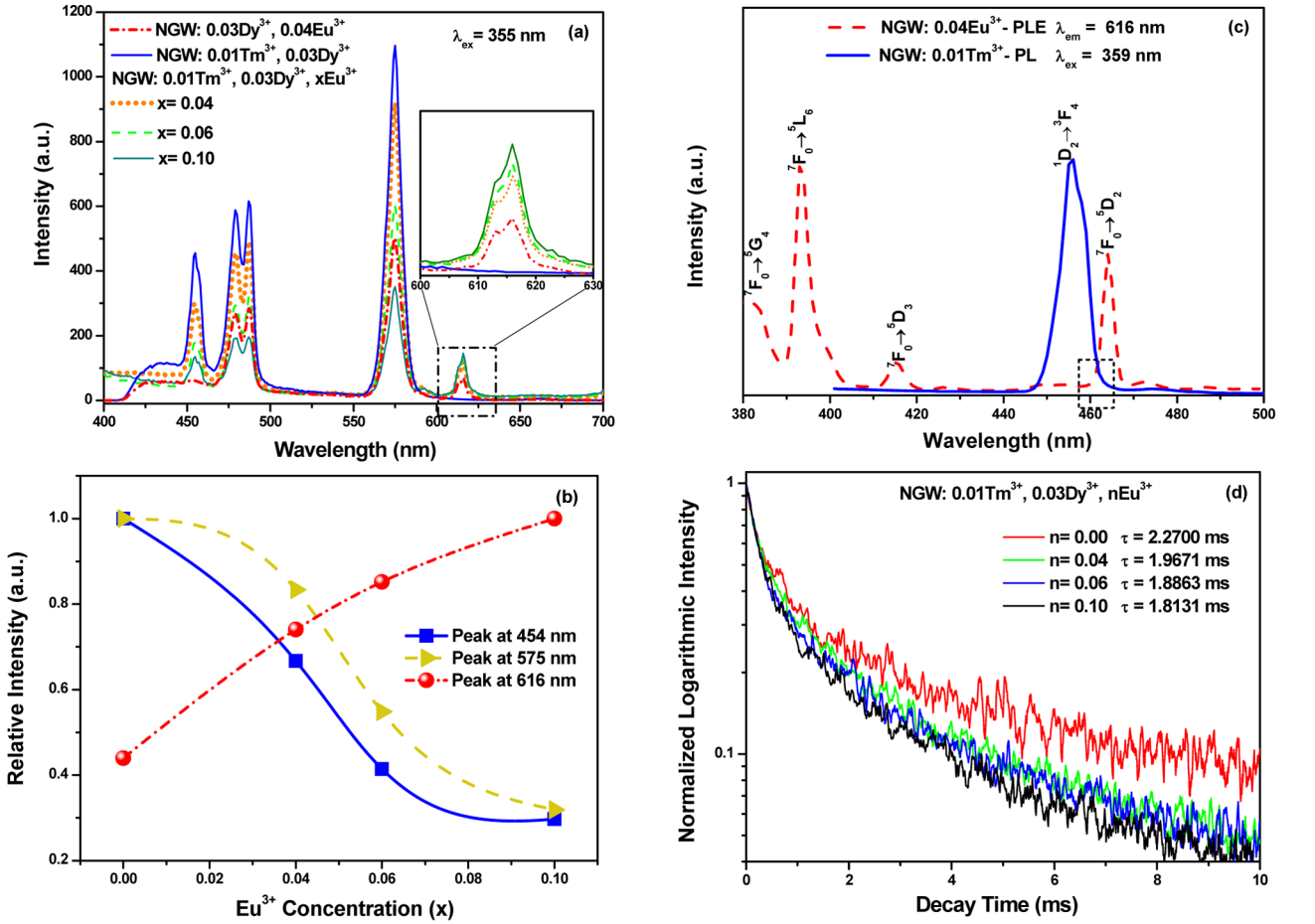

Figure 12. PL spectra for NGW:0.03Dy^{3+}, 0.04Eu^{3+}, NGW:0.01Tm^{3+}, 0.03Dy^{3+}, and NGW:0.01Tm^{3+}, 0.03Dy^{3+}, $x$$Eu^{3+}$ (x = 0.04, 0.06, 0.10) phosphors under 355 nm excitation (a); dependence of the emission intensity at different wavelengths on Eu^{3+} concentration (b); overlapping of Tm^{3+} PL spectrum for NGW:0.01Tm^{3+} and the Eu^{3+} PLE spectrum for NGW:0.04Eu^{3+} (c); decay curves for Tm^{3+} ions in NGW:Tm^{3+}, Dy^{3+}, Eu^{3+} samples (excited at 359 nm, monitored at 454 nm) (d).

Table 2. Luminescence Energy Transfer Rates and Efficiencies Calculated for NGW:0.01Tm^{3+}, 0.03Dy^{3+}, $x$$Eu^{3+}$Samples

	x = 0.04	x = 0.06	x = 0.10
α_1	0.2258	0.2476	0.2690
α_2	1.4149	1.4346	1.9559
η_1	0.4442	0.4670	0.4877
η_2	0.7016	0.7045	0.7648

decay curves. The fluorescence decay process of Dy^{3+} ions in NGW:0.03Dy^{3+}, $x$$Eu^{3+}$ phosphors is investigated by monitoring at 575 nm with irradiation of 353 nm. Assuming that electric multipolar interaction, the modificatory decay function of excited donors due to energy transfer to the acceptors is given by following equation[30]

$$I(t) = I_0(t)\exp[-4/3\pi\Gamma(1 - 3/S)n_A\alpha^{3/S}t^{3/S}] \quad (3)$$

where $I_0(t)$ characterizes the decay function of donors without the acceptors, n_A is the number of acceptor ions per unit volume, α is the rate constant for energy transfer, S = 6, 8, 10, the coefficient for dipole−dipole, dipole−quadrupole, and quadrupole−quadrupole interaction, respectively. From eq 3, it can be found that $\log\{-\ln[I(t)/I_0(t)]\}$ acts as a linear function of $\log(t)$ with a slope of $3/S$. In order to understand well the Dy^{3+}−Eu^{3+} energy transfer mechanism, we plotted the $\log\{-\ln[I(t)/I_0(t)]\}$ versus $\log(t)$ of Dy^{3+} in the NGW:0.03Dy^{3+}, $x$$Eu^{3+}$ phosphors as shown in Figure 6. As the results of linear fitting shown, the slopes are approximately 0.392, 0.368, 0.362, and 0.361 for NGW:0.03Dy^{3+}, $x$$Eu^{3+}$ samples with x = 0.02, 0.04, 0.06, and 0.10, respectively. Therefore, the calculated values of S are close to 8, indicating that energy transfer from Dy^{3+} to Eu^{3+} occurs via the electric dipole−quadrupole mechanism in the NGW host.

On the basis of Dexter's energy transfer formula of multipolar interaction and Reisfeld's approximation, the following equation can be used to analyze the potential mechanism[29,31,32]

$$I_{so}/I_s \propto C^{n/3} \quad (4)$$

where I_{so} is the intrinsic luminescence intensity of donors, and I_s is the luminescence intensity of donors in the presence of acceptors, and C is the doped concentration of acceptors. When the value of n is 6, 8, or 10, the interaction corresponds to dipole−dipole, dipole−quadrupole, or quadrupole−quadrupole, respectively. The I_{so}/I_s plots are illustrated in Figure 7, and the plots are used for linear fitting. It can be clearly seen that when n = 8, linear fitting result is the best, clearly implying the dipole−quadrupole interaction predominates in the energy transfer process between Dy^{3+} and Eu^{3+} ions, which is coincident with that analyzed above by the Inokuti−Hirayama (I−H) model.

3.3. Photoluminescence Properties of NaGd$(WO_4)_2$:Tm^{3+}, Dy^{3+} Phosphors. Figure 8 shows the PLE and PL spectra for NGW:0.01Tm^{3+} (a) and NGW:0.01Tm^{3+},

dx.doi.org/10.1021/ic501284y | Inorg. Chem. 2014, 53, 11457−11466

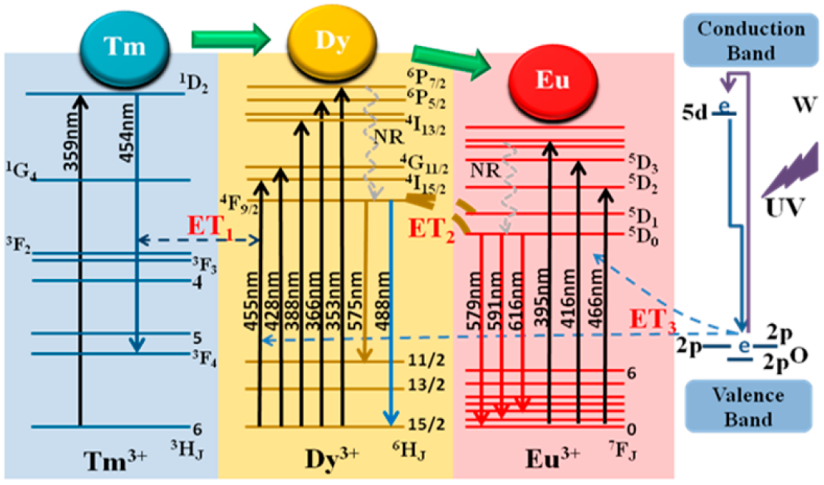

Figure 13. Schematic energy-level diagram showing the excitation and emission mechanism of NGW:Tm^{3+}, Dy^{3+}, Eu^{3+} phosphors (ET, energy transfer; NR, nonradiative).

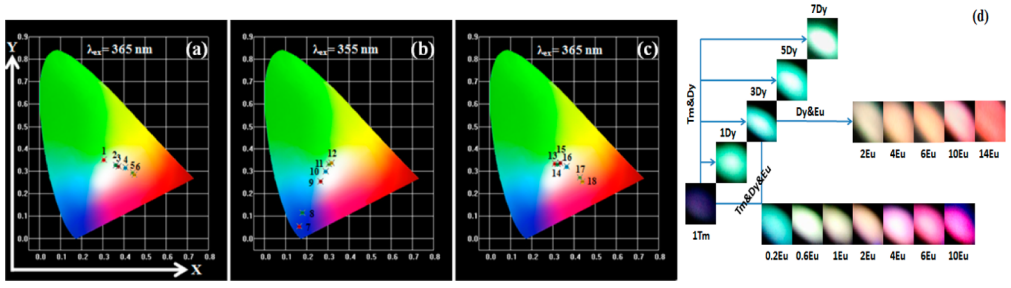

Figure 14. CIE chromaticity diagram (a, b, and c) and corresponding luminescence photographs (d) of NGW:Tm^{3+}, Dy^{3+}, Eu^{3+} phosphors.

Table 3. CIE Chromaticity Coordinates for NGW:Tm^{3+}, Dy^{3+}, Eu^{3+} Samples

label	sample	excitation/nm	CIE (x, y)	CC T/K
1	NGW:0.03Dy^{3+}	365	(0.306, 0.353)	6695
2	NGW:0.03Dy^{3+}, 0.02Eu^{3+}	365	(0.363, 0.328)	4139
3	NGW:0.03Dy^{3+}, 0.04Eu^{3+}	365	(0.375, 0.322)	3619
4	NGW:0.03Dy^{3+}, 0.06Eu^{3+}	365	(0.407, 0.318)	2567
5	NGW:0.03Dy^{3+}, 0.10Eu^{3+}	365	(0.442, 0.295)	1867
6	NGW:0.03Dy^{3+}, 0.14Eu^{3+}	365	(0.449, 0.284)	2168
7	NGW:0.01Tm^{3+}	359	(0.164, 0.054)	2178
8	NGW:0.01Tm^{3+}	355	(0.180, 0.116)	11437
9	NGW:0.01Tm^{3+}, 0.01Dy^{3+}	355	(0.266, 0.256)	15945
10	NGW:0.01Tm^{3+}, 0.03Dy^{3+}	355	(0.291, 0.301)	8411
11	NGW:0.01Tm^{3+}, 0.05Dy^{3+}	355	(0.306, 0.332)	6858
12	NGW:0.01Tm^{3+}, 0.07Dy^{3+}	355	(0.317, 0.337)	6238
13	NGW:0.01Tm^{3+}, 0.03Dy^{3+}, 0.002Eu^{3+}	365	(0.311, 0.335)	6560
14	NGW:0.01Tm^{3+}, 0.03Dy^{3+}, 0.006Eu^{3+}	365	(0.323, 0.333)	5947
15	NGW:0.01Tm^{3+}, 0.03Dy^{3+}, 0.01Eu^{3+}	365	(0.334, 0.338)	5422
16	NGW:0.01Tm^{3+}, 0.03Dy^{3+}, 0.04Eu^{3+}	365	(0.364, 0.322)	4040
17	NGW:0.01Tm^{3+}, 0.03Dy^{3+}, 0.06 Eu^{3+}	365	(0.427, 0.273)	1960
18	NGW:0.01Tm^{3+}, 0.03Dy^{3+}, 0.10Eu^{3+}	365	(0.441, 0.254)	4846

0.03Dy^{3+} (b) phosphors. In Figure 8a, it can be seen that the excitation spectrum of NGW:0.01Tm^{3+} shows a sharp absorption peak at 359 nm assigned to the $^3H_6 \rightarrow {}^1D_2$ transition of Tm^{3+}, which matches well with the UV-LED chips. However, we could not see a charge transfer band for WO_4^{2-} groups from 200 to 300 nm, proving the inexistence of the energy transfer from WO_4^{2-} groups to Tm^{3+} ions. Upon excitation at 359 nm, the NGW:0.01Tm^{3+} phosphor exhibits an intense blue emission assigned to the $^1D_2 \rightarrow {}^3F_4$ transition (454 nm), which could be a favorable candidate in blue phosphor for nUV-LEDs. Figure 8b presents the PLE and PL spectra of NGW:0.01Tm^{3+}, 0.03Dy^{3+} phosphor. When monitoring by the yellow emission of Dy^{3+} (575 nm) and blue emission of Tm^{3+} (454 nm), the PLE spectra of NGW:0.01Tm^{3+}, 0.03Dy^{3+} illustrate some absorption peaks corresponding to the characteristic transitions of Dy^{3+} and Tm^{3+}, respectively. With 359 nm excitation of Tm^{3+} ions, emission spectrum for NGW:0.01Tm^{3+}, 0.03Dy^{3+} phosphor is composed of several bands associated with the transitions of the $Tm^{3+}$and

dx.doi.org/10.1021/ic501284y | Inorg. Chem. 2014, 53, 11457−11466

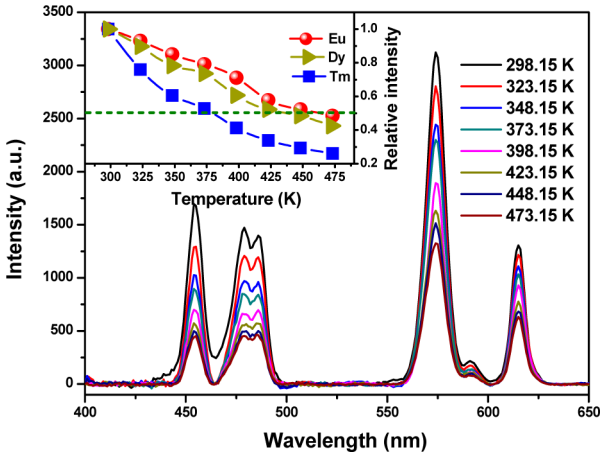

Figure 15. PL spectra of the NGW:Tm^{3+}, Dy^{3+}, Eu^{3+} phosphor excited at 365 nm with different temperatures. Inset shows relative PL intensities of Tm^{3+}, Dy^{3+}, and Eu^{3+} in the NGW host with raised temperatures.

Dy^{3+} ions from the $^1D_2$ and $^4F_{9/2}$ electronic levels, respectively. However, the emission intensities of Dy^{3+} ions at 478, 488, and 575 nm are very low (short dash dot line, Figure 8b). Alternatively, with $^6H_{15/2} \rightarrow {}^6P_{7/2}$ excitation of Dy^{3+} ions at 353 nm, the emission of Tm^{3+} ions at 454 nm is similarly too feeble (solid line, Figure 8b). That is because the energy transfer between Tm^{3+} and Dy^{3+} is weak if the intense excitation of either Tm^{3+} or Dy^{3+} ions is selected. Hence, it is necessary to select a suitable excitation wavelength for obtaining equal blue and yellow emissions. The red dash line in the PLE spectra shows the cross-sectional area of the excitation bands of both Tm^{3+} and Dy^{3+} ions with equal energy levels. Thus, the most effective excitation is estimated to this cross sectional area at 355 nm as the excitation wavelength to generate relative stronger emissions of Tm^{3+} as well as Dy^{3+} ions (short dot line, Figure 8b). Because the Tm^{3+} $^3H_6 \rightarrow {}^1D_2$ transition (359 nm) locates between the Dy^{3+} $^6H_{15/2} \rightarrow {}^6P_{7/2}$ transition (353 nm) and $^6H_{15/2} \rightarrow {}^6P_{5/2}$ transition (366 nm), and there is an overlap between them, one can distinctly observe that the $^6H_{15/2} \rightarrow {}^6P_{5/2}$ transition at 366 nm of Dy^{3+} is higher than the Dy^{3+} $^6H_{15/2} \rightarrow {}^4I_{13/2}$ transition at 388 nm, which is different from the PLE spectrum of single doping NGW with Dy^{3+} shown in Figures 3a and 8c, demonstrating the existence of energy transfer from Tm^{3+} to Dy^{3+} in NGW. In Figure 8c, we can markedly see a significant spectral overlap between the emission of Tm^{3+} and the excitation of Dy^{3+}. Accordingly, white light emission can be realized by combining the blue and yellow emissions of the Tm^{3+} and Dy^{3+} ions in a single host under UV light excitation.

A series of phosphors with fixed Tm^{3+} or Dy^{3+} concentrations were prepared to study the impact of doping concentration on the luminescence properties of phosphors. Figure 9 illustrates a series of emission spectra for NGW:0.01Tm^{3+}, $y$$Dy^{3+}$ (y = 0.00, 0.01, 0.03, 0.05, and 0.07) (a) and NGW:$z$$Tm^{3+}$, 0.03$Dy^{3+}$ (z = 0.00, 0.005, 0.01, 0.03, 0.05 and 0.07) (b) under UV excitation. With the doping concentration of Tm^{3+} fixed at 0.01, with increasing Dy^{3+} concentration, the emission intensities of the Dy^{3+} first increase to an optimum concentration at 0.03 and then decrease, whereas that of the Tm^{3+} decreases monotonically, reflecting the result of energy transfer from Tm^{3+} to Dy^{3+}. In addition, Figure 9b depicts the PL spectra of NGW:$z$$Tm^{3+}$, 0.03$Dy^{3+}$ phosphors with z varying from 0.00 to 0.07. Although the Dy^{3+} concentration is fixed, the emission intensity of Dy^{3+} ions demonstrably increased at a certain range, further proving the energy migration from Tm^{3+} to Dy^{3+} ions. However, the intensity of the Dy^{3+} emission first increases to a maximum at z = 0.01, then decreases due to the concentration quenching, during which the excitation energy is lost to the killer sites non-radiatively.[33] The concentration quenching of the Dy^{3+} emission is mainly due to the cross relaxation between neighboring Dy^{3+} ions which are in resonance of their energy levels due to the Dy^{3+} ($^4F_{9/2}$) + Dy^{3+} ($^6H_{15/2}$) → Dy^{3+} ($^6F_{3/2}$) + Dy^{3+} ($^6F_{11/2}$) transitions.[34] The above phenomena suggest that the energy transfer occurs from Tm^{3+} to Dy^{3+}. The possible energy transfer mechanism is shown in Figure 13. The energy difference between $^1D_2$ and $^3F_4$ of Tm^{3+} matches well with that between $^6H_{15/2}$ and $^4I_{15/2}$ of Dy^{3+}, which makes the energy migration from Tm^{3+} to Dy^{3+} efficient. Therefore, the luminescence intensities of various rare earth ions can be enhanced or quenched by the energy transfer from other codoped rare earth ions.[35] Those illustrate the occurrence of energy transfer from Tm^{3+} to Dy^{3+} when they are codoped in the NGW host and provide a necessary condition for synthesizing the single phase full-color phosphors. The energy transfer efficiencies η_{Tm-Dy} are calculated using eq 1, characterized as a function of Dy^{3+} concentrations, and are shown in Figure 10. The efficiency η_{Tm-Dy} increases gradually with the increase of Dy^{3+} concentration and approximately reaches 82% at y = 0.07.

According to Dexter's energy transfer expressions of multipolar interaction, we also employ eq 4 to analyze the potential mechanism of energy migration from Tm^{3+} to Dy^{3+} ions. Figure 11 has illustrated the plots of I_{so}/I_s of Tm^{3+}, and the plots are used for linear fitting, which are best fitted at n = 8, indicating the energy transfer mechanism via a dipole−quadrupole interaction between the Tm^{3+} to Dy^{3+} ions.

3.4. Photoluminescence Properties of NaGd(WO$_4$)$_2$:Tm^{3+}, Dy^{3+}, Eu^{3+} Phosphors. Materials doped only with Tm^{3+} and Dy^{3+} ions exhibited cool white light. Tridoping Eu^{3+} ions and increasing the Eu^{3+} concentration can shift the color of the emission to warm white, with intermediate yellowish and red colors. The PL spectra of the prepared NGW:Tm^{3+}, Dy^{3+}, Eu^{3+} phosphors are presented in Figure 12a. Upon excitation at 355 nm, the red emission of the sample doped only with 0.03Dy^{3+} and 0.04Eu^{3+} is very low (red short dash dot line, Figure 12a). When tridoping 0.01Tm^{3+} ions, the red emission intensity is approximately twice as high as that of NGW:0.03Dy^{3+}, 0.04Eu^{3+} phosphor (orange short dot line, Figure 12a). This phenomenon is a result of the energy migration from Tm^{3+} to Eu^{3+} through Dy^{3+} ions. Moreover, by comparison with the emissions of NGW:0.01Tm^{3+}, 0.03Dy^{3+}, $x$$Eu^{3+}$ (x varying from 0.00 to 0.10), it can be clearly seen that although the Tm^{3+} and Dy^{3+} concentrations are fixed, the emission intensities for Tm^{3+} as well as Dy^{3+} ions demonstrably decreased with the doping of Eu^{3+} ions, further proving the energy transfer from Tm^{3+} to Eu^{3+} ions via Dy^{3+}. The relative emission intensities of Tm^{3+} ions at 454 nm, Dy^{3+} ions at 575 nm, and Eu^{3+} ions at 616 nm as a function of Eu^{3+} concentration are shown in Figure 12b. In Figure 12c, it is found that the excitation bands of Eu^{3+} overlap to some extent in the range 450−465 nm with the emission peak of Tm^{3+}, which suggests the existence of energy migration between Tm^{3+} and Eu^{3+} ions. Figure 12d shows the luminescence decays of the NGW:Tm^{3+}, Dy^{3+}, Eu^{3+} microcrystals under excitation by $^1D_2 \rightarrow {}^3F_4$ transition of Tm^{3+} ions with a wavelength at 454 nm. From Figure 12d, one can see that the decay behavior of Tm^{3+} can be best fitted to the double-exponential equation

dx.doi.org/10.1021/ic501284y | Inorg. Chem. 2014, 53, 11457−11466

$$I = I_0 + A_1 \exp(-t/\tau_1) + A_2 \exp(-t/\tau_2) \quad (5)$$

Also, the average lifetime values are calculated using

$$\tau_{av} = (A_1\tau_1^2 + A_2\tau_2^2)/(A_1\tau_1 + A_2\tau_2) \quad (6)$$

On the basis of eq 6 presented above, we calculated the decay times of Tm^{3+} ions. From Figure 12d, it can be seen that the decay times for Tm^{3+} ions are shortened by increasing the Eu^{3+} concentration. This performance is especially useful for confirming the effective energy migration process. In order to further validate the effectiveness of the occurred energy migration, we have calculated energy transfer rates and energy transfer efficiencies estimated from measured lifetimes. Presuming that in case of tridoped samples there are two energy transfer processes issuing in increment of Eu^{3+} emission, between Tm^{3+} and Dy^{3+} ions (ET_1) and Dy^{3+} and Eu^{3+} ions (ET_2), energy transfer processes can be analyzed from the following equations:[36,37]

$$\xi = dN_1(t)/dt = -k_1N_{10} = -\tau_{Tm}^{-1}N_{10} \quad (7)$$

$$\xi = dN_1(t)/dt = -(k_1 + \alpha_1)N_{10} = -\tau_{Tm-Dy-Eu}^{-1}N_{10} \quad (8)$$

Here ξ is the luminescence rate, $N_1(t)$ is the total population of electrons from $Tm^{3+1}D_2$ level, N_{10} is the number densities of electrons from $Tm^{3+1}D_2$ level when $t = 0$, α_1 is the rate constant of energy transfer from Tm^{3+} ions, τ_{Tm} is the luminescence lifetime of Tm^{3+} ions in absence of Dy^{3+} and Eu^{3+} ions, equal to 3.5392 ms, and $\tau_{Tm-Dy-Eu}$ is luminescence lifetime of Tm^{3+} ions in the presence of Dy^{3+} and Eu^{3+} ions. From eqs 7 and 8, it is possible to calculate the rate constant α_1 of energy transfer from Tm^{3+} to Dy^{3+} ions:

$$\alpha_1 = (\tau_{Tm} - \tau_{Tm-Dy-Eu})/\tau_{Tm-Dy-Eu}\tau_{Tm} \quad (9)$$

Also, the energy transfer efficiency η_1 from Tm^{3+} to Dy^{3+} ions follows:

$$\eta_1 = 1 - \tau_{Tm-Dy-Eu}/\tau_{Tm} \quad (10)$$

Similarly, the rate constant α_2 and efficiency η_2 of energy transfer from Dy^{3+} to Eu^{3+} ions can be calculated by

$$\alpha_2 = (\tau_{Dy} - \tau_{Dy-Tm-Eu})/\tau_{Dy-Tm-Eu}\tau_{Dy} \quad (11)$$

$$\eta_2 = 1 - \tau_{Dy-Tm-Eu}/\tau_{Dy} \quad (12)$$

where τ_{Dy} is the luminescence lifetime of only doping Dy^{3+} ions, equal to 1.6621 ms, and $\tau_{Dy-Tm-Eu}$ is luminescence lifetime of Dy^{3+} ions in the presence of Tm^{3+} and Eu^{3+} ions.

Energy transfer rates and efficiencies calculated are presented in Table 2. It can be seen that energy transfer rate between Dy^{3+} and Eu^{3+} ions is almost 6 times faster than that between Tm^{3+} and Dy^{3+} ions. Also, energy transfer efficiency is 1.5 times higher between Dy^{3+} and Eu^{3+} ions due to the similarity between the energies of their excited states.

A schematic model proposed for the probable methods of energy transfer in NGW:Tm^{3+}, Dy^{3+}, Eu^{3+} phosphors is shown in Figure 13. During the excitation process, the electrons situated at oxygen 2p states absorb energies of photons from UV. As a consequence of this phenomenon, the energetic electrons are promoted to tungsten 5d states located near the conductor band.[38] When the electrons fall back to lower energy states again via blue emission and energy transfer to Dy^{3+} and Eu^{3+} ions, some energy is lost by cross relaxation. Furthermore, the energy transfer also occurs between Tm^{3+} and Eu^{3+} through Dy^{3+} ions.

3.5. Codoping $NaGd(WO_4)_2$ with Tm^{3+}, Dy^{3+}, and Eu^{3+} for Single-Phased White Light Emission. The energy transfer among activator ions (Tm^{3+}, Dy^{3+}, Eu^{3+}) offers an approach to tune emission colors. Therefore, we have studied the Commission Internationale de L'Eclairage (CIE) values of the suite of NGW:Tm^{3+}, Dy^{3+}, Eu^{3+} phosphors. The CIE chromaticity coordinates for the phosphors excited at different wavelengths were determined on the basis of their corresponding PL spectrum, and are represented in the CIE diagram of Figure 14 with the data given in Table 3. For the NGW:Dy^{3+}, Eu^{3+} phosphors, the Dy^{3+} doping concentration is fixed at 0.03, as the concentration of Eu^{3+} increased from 0.00 to 0.14. It can be seen that when excited at 365 nm, the trend of their color tones changes from cool white to red by adjusting the doping concentration of Eu^{3+}; the corresponding chromaticity coordinates are presented in Figure 14a (point 1−6). Especially, there is a point at (0.363, 0.328) close to standard white light (0.33, 0.33) with a lower correlated color temperature of 4139 K. In addition, the CIE chromaticity coordinates with varied color tones of NGW:Tm^{3+}, Dy^{3+} samples have been calculated and shown in Figure 14b. The NGW:0.01Tm^{3+} phosphor excited by 359 or 355 nm exhibited bright blue emission (point 7 and 8 in Figure 14b), applying potentially in blue LEDs. When codoping Dy^{3+} ions, samples emit light entirely in the white region with unfavorable high correlated color temperature (>5000 K) restricting their application in solid state lighting (point 9−12). Therefore, tridoping Eu^{3+} ions are employed to shift the color of the emissions to warm white, by providing red colors, which are shown in Figure 14c. Almost all of the white light region can be observed by appropriate tuning of the dopant concentration of Tm^{3+}, Dy^{3+}, and Eu^{3+} as well as the excitation wavelengths. The corresponding luminescence photographs of all the prepared phosphors are shown in Figure 14d.

3.6. Thermal Stability Properties of $NaGd(WO_4)_2$:Tm^{3+}, Dy^{3+}, Eu^{3+}. For the application in solid-state lighting, especially high power LEDs, the thermal stability property of phosphors is one of the crucial technological parameters. The thermal stability of $NaGd(WO_4)_2$:0.01Tm^{3+}, 0.03Dy^{3+}, 0.04Eu^{3+} (sample 16) is evaluated according to the dependence of the emission spectra under 365 nm excitation on the temperatures from 298.15 to 473.15 K, as shown in Figure 15. The PL relative intensities as a function of temperature are plotted in the inset of Figure 15. The PL intensity from the three emission centers Tm^{3+}, Dy^{3+}, Eu^{3+} decreases to 73.9%, 57.5%, and 51.6% (473.15 K) of the initial value (298.15 K), respectively. With additional research, we are looking into ways of increasing the stability for application in LED technologies.

4. CONCLUSIONS

In summary, series novel color-tunable single-component $NaGd(WO_4)_2$:Tm^{3+}, Dy^{3+}, Eu^{3+} white phosphors were prepared by one-step hydrothermal method at 180 °C for 20 h. In the case of Eu^{3+} and Dy^{3+} codoped systems as well as $NaGd(WO_4)_2$:Tm^{3+}, Dy^{3+} phosphors, the efficient and strong energy transfer process occurs via the dipole−quadrupole mechanism. In addition, in $NaGd(WO_4)_2$:Tm^{3+}, Dy^{3+}, Eu^{3+} phosphors, the rates and efficiencies of energy transfers between Tm^{3+} and Dy^{3+} as well as Dy^{3+} and Eu^{3+} are calculated. Those single-component phosphors exhibit abundant color-tunable emissions besides warm white light with low correlated color temperature via effective energy migration process in the $NaGd(WO_4)_2$ host.

dx.doi.org/10.1021/ic501284y | Inorg. Chem. 2014, 53, 11457−11466

Almost all of the prepared phosphors could find applications in WLEDs.

AUTHOR INFORMATION

Corresponding Author

*E-mail: liuguixia22@163.com. Phone: +86-431-85582574. Fax: +86-431-85383815

Notes

The authors declare no competing financial interest.

ACKNOWLEDGMENTS

This work was supported by the National Natural Science Foundation of P. R. China (NSFC) (Grant 51072026, 50972020) and the Development of Science and Technology Plan Projects of Jilin Province (Grant 20130206002GX).

REFERENCES

(1) Hashimoto, T.; Wu, F.; Speck, J. S.; Nakamura, S. *Nat. Mater.* **2007**, *6*, 568−571.

(2) Suehiro, T.; Hirosaki, N.; Xie, R. J. *ACS Appl. Mater. Interfaces* **2011**, *3*, 811−816.

(3) Nakamura, S.; Mukai, T.; Senoh, M. *Appl. Phys. Lett.* **1994**, *64*, 1687−1689.

(4) Im, W. B.; Brinkley, S.; Hu, J.; Mikhailovsky, A.; DenBaars, S. P.; Seshadri, R. *Chem. Mater.* **2010**, *22*, 2842−2849.

(5) Guo, N.; Lü, W.; Jia, Y.; Lv, W.; Zhao, Q.; You, H. *ChemPhysChem* **2013**, *14*, 192−197.

(6) Liu, X.; Hou, W.; Yang, X.; Liang, J. *CrystEngComm* **2014**, *16*, 1268−1276.

(7) Wu, L.; Zhang, Y.; Gui, M.; Lu, P.; Zhao, L.; Tian, S.; Kong, Y.; Xu, J. *J. Mater. Chem.* **2012**, *22*, 6463−6470.

(8) Luwang, M. N.; Ningthoujam, R. S.; Srivastava, S. K.; Vatsa, R. K. *J. Mater. Chem.* **2011**, *21*, 5326−5337.

(9) Wen, D.; Shi, J. *Dalton Trans.* **2013**, *42*, 16621−16629.

(10) Singh, N. S.; Sahu, N. K.; Bahadur, D. *J. Mater. Chem. C* **2014**, *2*, 548−555.

(11) Geng, D.; Shang, M.; Zhang, Y.; Lian, H.; Cheng, Z.; Lin, J. *J. Mater. Chem. C* **2013**, *1*, 2345−2353.

(12) Liu, H.; Luo, Y.; Mao, Z.; Liao, L.; Xia, Z. *J. Mater. Chem. C* **2014**, *2*, 1619−1627.

(13) Zhu, G.; Xin, S.; Wen, Y.; Wang, Q.; Que, M.; Wang, Y. *RSC Adv.* **2013**, *3*, 9311−9318.

(14) Sava, D. F.; Rohwer, L. E. S.; Rodriguez, M. A.; Nenoff, T. M. *J. Am. Chem. Soc.* **2012**, *134*, 3983−3986.

(15) Sava Gallis, D. F.; Rohwer, L. E. S.; Rodriguez, M. A.; Nenoff, T. M. *Chem. Mater.* **2014**, *26*, 2943−2951.

(16) Falcaro, P.; Furukawa, S. *Angew. Chem.* **2012**, *51*, 8431−8433.

(17) Shang, M.; Geng, D.; Kang, X.; Yang, D.; Zhang, Y.; Lin, J. *Inorg. Chem.* **2012**, *51*, 11106−11116.

(18) Pavitra, E.; Raju, G. S. R.; Park, W.; Yu, J. S. *New J. Chem.* **2014**, *38*, 163−169.

(19) Som, S.; Mitra, P.; Kumar, V.; Kumar, V.; Terblans, J. J.; Swart, H. C.; Sharma, S. K. *Dalton Trans.* **2014**, *43*, 9860−9871.

(20) Wang, X. F.; Yan, X. H.; Bu, Y. Y.; Zhen, J.; Xuan, Y. *Appl. Phys. A: Mater. Sci. Process.* **2013**, *112*, 317−322.

(21) Zhou, P.; Zhu, Y.; Xu, W.; Xu, L.; Song, H. *Opt. Express* **2013**, *21*, 25744−25751.

(22) Zhang, Y.; Geng, D.; Shang, M.; Zhang, X.; Li, X.; Cheng, Z.; Lian, H.; Lin, J. *Dalton Trans.* **2013**, *42*, 4799−4808.

(23) Li, G.; Li, C.; Zhang, C.; Cheng, Z.; Quan, Z.; Peng, C.; Lin, J. *J. Mater. Chem.* **2009**, *19*, 8936−8943.

(24) Zhang, X.; Zhou, L.; Pang, Q.; Shi, J.; Gong, M. *J. Phys. Chem. C* **2014**, *118*, 7591−7598.

(25) Xia, Z.; Zhuang, J.; Meijerink, A.; Jing, X. *Dalton Trans.* **2013**, *42*, 6327−6336.

(26) Lin, J.; Su, Q.; Wang, S.; Zhang, H. *J. Mater. Chem.* **1996**, *6*, 265−269.

(27) Zhang, J.; Hong, G. *J. Solid State Chem.* **2004**, *177*, 1292−1296.

(28) Cao, C. Y.; Yang, H. K.; Chuang, J. W.; Moon, B. K.; Choi, B. C.; Jeong, J. H.; Kim, K. H. *J. Mater. Chem.* **2011**, *21*, 10342−10347.

(29) Blasse, G. *Philips Res. Rep.* **1969**, *24*, 131−144.

(30) Ohashi, H.; Ii, N. *J. Japan. Assoc. Mineral., Petrol. Econ. Geol.* **1978**, *73*, 267−272.

(31) Reisfeld, R.; Greenberg, E.; Velapoldi, R.; Barnett, B. *J. Chem. Phys.* **1972**, *56*, 1698−1705.

(32) Dexter, D. L.; Schulman, J. H. *J. Chem. Phys.* **1954**, *22*, 1063−1070.

(33) Blasse, G.; Grabmaier, B. C. *Luminescent Materials, Energy Transfer*; Springer: Berlin, 1994.

(34) Yu, C. C.; Liu, X. M.; Yu, M.; Lin, C. K.; Li, C. X.; Wang, H.; Lin, J. *J. Solid State Chem.* **2007**, *180*, 3058−3065.

(35) Shang, M.; Li, G.; Kang, X.; Yang, D.; Geng, D.; Lin, J. *ACS Appl. Mater. Interfaces* **2011**, *3*, 2738−2746.

(36) Arai, Y.; Yamashidta, T.; Suzuki, T.; Ohishi, Y. *J. Appl. Phys.* **2009**, *105*, 083105−083106.

(37) Grzyb, T. *RSC Adv.* **2014**, *4*, 2590−2595.

(38) Sczancoski, J. C.; Cavalcante, L. S.; Marana, N. L.; Silva, R. O.; Tranquilin, R. L.; Joya, M. R.; Pizani, P. S.; Varela, J. A.; Sambrano, J. R.; Siu, L. M.; Longo, E.; Andrés, J. *Curr. Appl. Phys.* **2010**, *10*, 614−624.